Available online at www.sciencedirect.com
ScienceDirect
Trans. Nonferrous Met. Soc. China 32(2022) 2746−2756
Transactions of Nonferrous Metals Society of China
www.tnmsc.cn

Lithium and manganese extraction from manganese-rich slag originated from pyrometallurgy of spent lithium-ion battery

Guo-xing REN[1], Cai-bin LIAO[2], Zhi-hong LIU[1], Song-wen XIAO[2]

1. School of Metallurgy and Environment, Central South University, Changsha 410083, China;
2. Changsha Research Institute of Mining & Metallurgy Co., Ltd., Changsha 410012, China

Received 19 July 2021; accepted 31 December 2021

Abstract: Mn and Li were selectively extracted from the manganese-rich slag by sulfation roasting−water leaching. The extraction mechanisms of Mn and Li were investigated by means of XRD, TG−DSC, and SEM−EDS. 73.71% Mn and 73.28% Li were leached under optimal experimental conditions: acid concentration of 82 wt.%, acid-to-slag mass ratio of 1.5:1, roasting temperature of 800 °C, and roasting time of 2 h. During the roasting process, the manganese-rich slag first reacted with concentrated sulfuric acid, producing $MnSO_4$, $MnSO_4·H_2O$, $Li_2Mg(SO_4)_2$, $Al_2(SO_4)_3$, and H_4SiO_4. With the roasting temperature increasing, H_4SiO_4 and $Al_2(SO_4)_3$ decomposed successively, resulting in generation of mullite and spinel. The mullite formation aided in decreasing the leaching efficiencies of Al and Si, while increasing the Li leaching efficiency. The formation of spinel, however, decreased the leaching efficiencies of Mn and Li.
Key words: spent lithium-ion battery; manganese-rich slag; sulfation roasting; manganese recovery; lithium recovery

1 Introduction

In recent years, lithium-ion battery (LIB) industry has become one of the rapidest expanding sectors in the world, driven mostly by the mass production of electric vehicles [1,2]. Generally speaking, the mean lifetimes of the LIBs used in electric vehicles are only 3−5 years; as a result, large amounts of end-of-life LIBs will be generated in the future, with the prediction that the mass of discarded LIBs is estimated to reach 11 million tons by 2030 worldwide [3]. Spent LIBs contain plenty of valuable metals, such as Cu, Co, Ni, Mn, and Li, together with plenty of toxic and hazardous contaminants [4−6]. Therefore, the recycling and treatment of spent LIBs have attracted wide interests in the view of the economic benefits and environmental protection.

The commercial technologies for recovering valuable metals from spent LIBs mainly include both single and combined mechanical, hydro-metallurgical and pyrometallurgical process [7−10]. Comparatively, the pyro-hydrometallurgical process is simpler and higher in efficiency, which can treat various types of batteries [11,12]. In this process, organic diaphragm materials, metallic aluminum foil, and graphite powders in the batteries are used as reducing agents, and energy sources. Valuable metals such as Co, Ni and Cu are concentrated into an alloy phase, and can be further separated by a hydrometallurgical method, while Li, Mn, and Al in batteries are fixed in the slag phase [7−9]. Due to the difference in the types of LIBs and the kind of added flux, the slag includes: $CaO–Al_2O_3$ binary [13], $CaO–SiO_2–Al_2O_3$ ternary [14], $FeO–SiO_2–Al_2O_3$ ternary [8], $SiO_2–Al_2O_3–Li_2O$ ternary [15], $MnO–SiO_2–Al_2O_3$ ternary [7,16,17],

Corresponding author: Zhi-hong LIU, Tel: +86-13873117863, E-mail: zhliu@csu.edu.cn;
Song-wen XIAO, Tel: +86-13973132417, E-mail: swinxiao@126.com
DOI: 10.1016/S1003-6326(22)65981-8

$CaO–FeO–SiO_2–Al_2O_3$ quaternary [8] and $CaO–SiO_2–Al_2O_3–Li_2O$ quaternary [13] systems.

To date, lithium in the slag originated from pyrometallurgy of spent lithium-ion batteries has not been recovered effectively [6,18−20]. One reason is that the content of lithium in the slag is low. The other reason is that the slurry obtained after routine acid leaching is difficult to filter due to the formation of silica gel (H_4SiO_4), resulting from the slags predominantly consisting of various aluminosilicates [7]. Recently, some studies have been conducted to develop a more practical method of extracting lithium from pyrometallurgical slag, including chlorination roasting [21], calcium chloride roasting [22], and sodium sulfate roasting followed by water leaching [23]. However, all of these methods have been focused on the recovery of lithium from simulated $CaO–SiO_2–Al_2O_3$ slag systems [21−23], which cannot reflect the technological progress in the development of LIB industry and the more complex compositions in the practical slag.

The $MnO–SiO_2–Al_2O_3$ slag has been viewed as the more suitable slag system for the smelting of automotive LIBs, due to the fact that the lithium nickel/cobalt/manganese oxide (NCM) battery with high Mn content has accounted for the largest share of the global automotive LIB market, resulting from its higher energy density and more reasonable cost [24−26]. Therefore, recovering Li and Mn from the $MnO–SiO_2–Al_2O_3$ slag has great significance.

In our previous study, we proposed a method for Li and Mn extraction from the $MnO–SiO_2–Al_2O_3$ slag by co-roasting with concentrated sulfuric acid. Even though purer leachate bearing manganese and lithium can be obtained, only 44.30% of Mn and 50.28% of Li from the manganese-rich slag were leached, which is far away from the commercial implementation [7]. In this work, in order to effectively improve the leaching efficiencies of manganese and lithium and propel this method toward commercial implementation, roasting parameters including roasting time, acid/slag ratio, and roasting temperature were systematically investigated. More importantly, the extraction mechanisms of Mn and Li in the slag were also investigated in details by means of TG−DSC, SEM−EDS, and XRD.

2 Experimental

2.1 Raw materials

The manganese-rich slag produced by smelting reduction of spent LIBs in a dc electric arc furnace, was used as the raw materials in this study. The chemical composition of the slag is given in Table 1. According to the SEM images and element distributions of the manganese-rich slag presented in Fig. 1, it was found that the manganese-rich slag mainly consists of Mn_2SiO_4 (tephroite), $Mn(Mg)Al_2O_4$ (spinel) and $LiAlSiO_4$. All chemical reagents for experiments were of analytical grade and de-ionized water was used in the leaching and diluting process.

Table 1 Composition of manganese-rich slag in this study (wt.%)

Li_2O	Na_2O	K_2O	MnO	MgO
2.83	0.36	1.43	33.01	1.06

SiO_2	Al_2O_3	Cu	Co	Ni	Fe
21.93	30.39	0.18	0.12	0.03	0.38

2.2 Experimental procedure

The manganese-rich slag was first crushed and ground before the experiments so that 90% of them would pass below 0.074 mm, and then mixed with sulfuric acid according to desired mass ratios. The mixtures were then heated at a determined temperature (200−800 °C) for a required time (2−8 h) in a muffle furnace. After roasting, the roasted samples were taken out and ground into powders using an agate mortar. In order to evaluate the effect of roasting on leaching, leaching experiments were carried out with certain leaching temperature (60 °C), leaching time (4 h), stirring speed (200 r/min) and solid/liquid (S/L) ratio (1:10 g/mL). After leaching, a filtration step was performed to collect the leaching residue. The leaching efficiencies (E) of Mn, Li, Al and Si were calculated as follows:

$$E = \left(1 - \frac{c_{i,s} \cdot m_s}{c_{i,0} \cdot m_0}\right) \times 100\% \quad (1)$$

where m_0 and m_s are the total masses of the manganese-rich slag and the residues after leaching, respectively; $c_{i,0}$ and $c_{i,s}$ are the contents of the

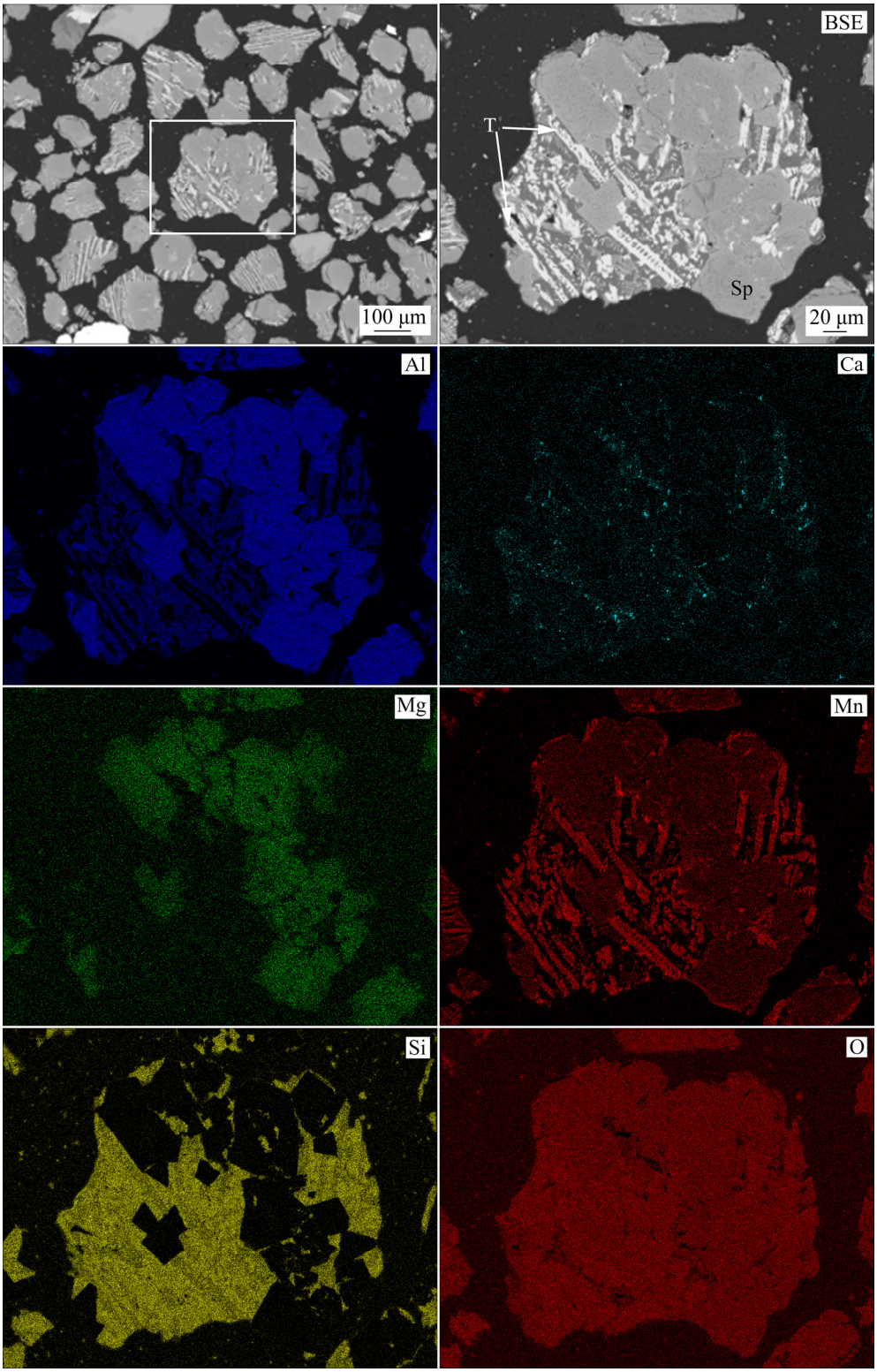

Fig. 1 Microstructure and elemental distributions of manganese-rich slag (T−Tephroite; Sp−Spinel)

element i in the manganese-rich slag and the residues after leaching, respectively.

The manganese-rich slag and roasted residues were analyzed with X-ray diffraction (XRD, D8 advance, Bruker) for the identification of the crystalline phases. Microstructure observation and composition identification of roasted residues were conducted by SEM with EDS (SEM−EDS, JSM−6490LV, JEOL Ltd.). The thermal analysis of the roasting process was conducted by thermal

gravimetry and differential scanning calorimetry (TG−DSC, STA 449F3, NETZSCH) at a heating rate of 10 °C/min in an air atmosphere. The chemical components of the leachate and Li in the leaching residue were analyzed by atomic absorption spectroscopy (AAS, TAS−990 Super, Beijing Purkinje General). The contents of Mn, Si and Al in the leaching residue were determined using ammonium ferrous sulfate titration, gravimetry by alkali fusion, and the EDTA volumetric method, respectively.

3 Results and discussion

3.1 Roasting−leaching

3.1.1 Effect of acid concentration

To investigate the effects of acid concentration on the leaching efficiencies of Mn and Li, the acid concentration was varied from 74 to 98 wt.%, and the acid-to-slag mass ratio, roasting temperature and roasting time were fixed at 1.0:1, 800 °C and 2 h, respectively. The results are presented in Fig. 2(a). As it can be seen, increasing the sulfuric acid concentration from 74 to 82 wt.% slightly increased the leaching efficiency of Mn from 62.29% to 65.22% and for Li from 74.19% to 74.33%. However, the Li leaching efficiency decreased significantly at acid concentrations higher than 82 wt.%. Thus, 82 wt.% was taken as the optimal condition for the Mn and Li leaching.

3.1.2 Effect of roasting temperature

The effect of different roasting temperatures ranging from 200 to 800 °C on the leaching efficiencies of Mn and Li was studied with an acid-to-slag mass ratio of 1.0:1, acid concentration of 82 wt.%, and a roasting time of 2 h. The results are depicted in Fig. 2(b). As observed, the roasting temperature has a significant impact on the extraction of Mn and Li from the Mn-rich slag. The leaching efficiencies of Li, Mn, Al, and Si decreased significantly as the roasting temperature increased from 200 to 500 °C. Although 95.99% of Li and 66.29% of Mn were leached at 200 °C, the leaching efficiencies of Al and Si also reached

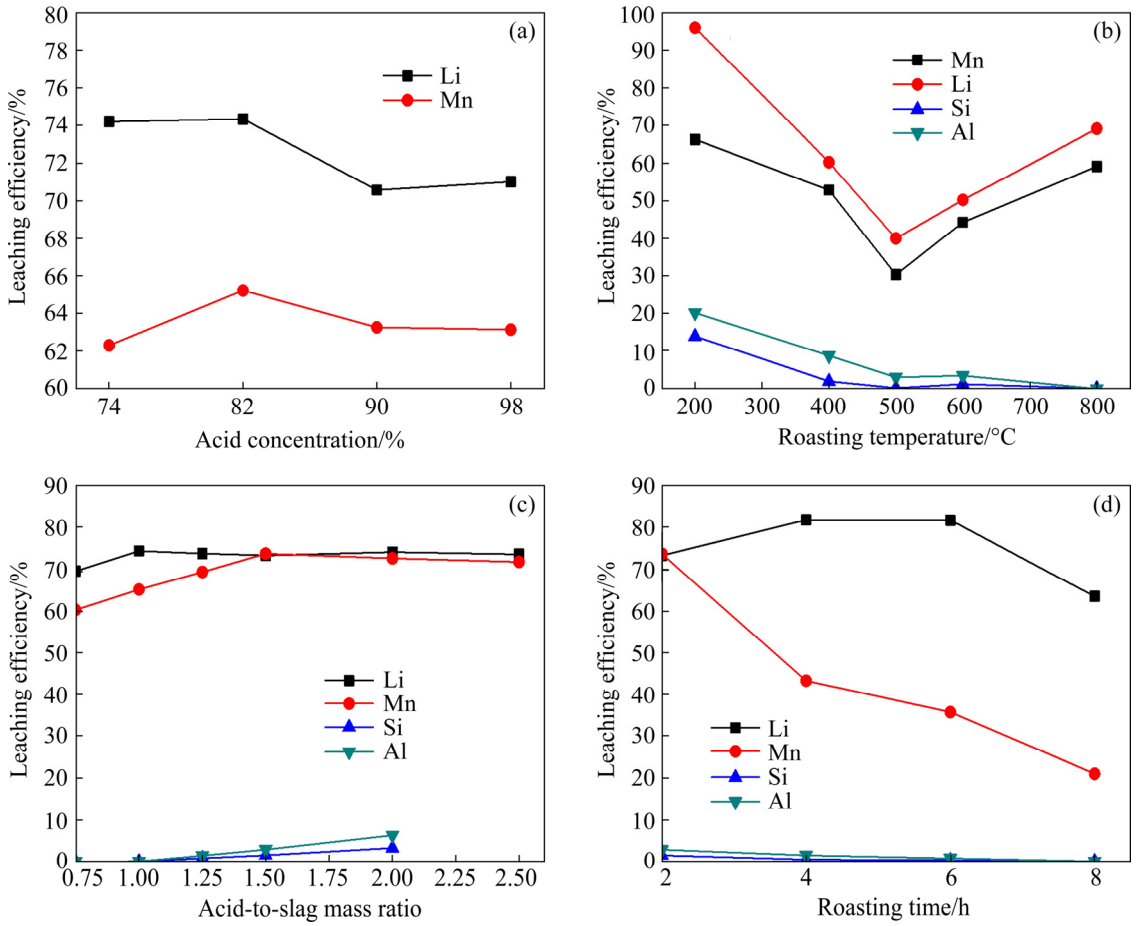

Fig. 2 Influence of different factors on leaching efficiencies of Mn, Li, Si, and Al: (a) Acid concentration; (b) Roasting temperature; (c) Acid-to-slag mass ratio; (d) Roasting time

20.12% and 13.84%, respectively, leading to the problem of filtering. A further increase in roasting temperature obviously increased the leaching efficiencies of Li and Mn. Conversely, the leaching rates of Al and Si decreased further. When the roasting temperature reached 800 °C, the leaching rates of Al and Si were only 0.01% and 0.07%, respectively. Therefore, the appropriate roasting temperature in this study was 800 °C.

3.1.3 Effect of acid-to-slag mass ratio

Figure 2(c) shows the effect of acid-to-slag mass ratio on the leaching of different metals under roasting conditions of acid concentration 82 wt.%, roasting temperature 800 °C, and roasting time 2 h. It can be seen that the leaching efficiency of Mn increased with the acid-to-slag mass ratio below 1.5:1, and then kept almost constant above this acid-to-slag mass ratio. The Li leaching efficiency remarkably increased with the acid-to-slag mass ratio increasing from 0.75:1 to 1.0:1, and remained almost constant above this acid-to-slag mass ratio. Therefore, the suitable acid-to-slag mass ratio was 1.5:1.

3.1.4 Effect of roasting time

Fixing the acid-to-slag mass ratio of 1.5:1, sulfuric acid concentration of 82 wt.%, and roasting temperature of 800 °C, the influence of roasting time on leaching efficiency was studied in detail. The result is shown in Fig. 2(d). As the roasting time increased from 2 to 8 h, the Mn leaching efficiency dropped rapidly from 73.71% to 21.01%. The Li leaching efficiency increased gradually from 73.28% to 81.72% when the roasting time increased from 2 to 6 h. However, the leaching efficiency of Li decreased when the roasting time was more than 6 h. Thus, the favorable roasting time is 2 h.

3.2 Roasting mechanism

To reveal the roasting reaction mechanisms of the manganese-rich slag with concentrated acid, the phase evolutions and microstructure changes of the slags at various roasting temperatures were investigated via HSC simulating calculation, XRD, TG−DSC and SEM−EDS.

3.2.1 Theoretical analysis of roasting process

In this study, the manganese-rich slag was roasted with H_2SO_4, and the possible reactions can be summarized in Table 2. Relationships between standard Gibbs free energy changes of the reactions (Δ_rG^{Θ}) and temperature are presented in Fig. 3 using HSC Chemistry version 6.0 software. It can be seen that the values of Δ_rG^{Θ} in Reactions (2)−(7) are all negative over the temperature range from 0 to 700 °C, indicating that $MnSO_4$ and Li_2SO_4 can be obtained first along with main by-products of $Al_2(SO_4)_3$ and H_4SiO_4 during heating the mixture. With the temperature increasing, the values of Δ_rG^{Θ} for Reactions (8)−(12) gradually decrease. As a result, the values of Δ_rG^{Θ} for Reactions (8) and (9) are observed to be negative first, which means that the H_4SiO_4 and $Al_2(SO_4)_3$ will be thus decomposed prior to the sulfates of Mn and Li in thermodynamic view. Therefore, it is possible to selectively extract Mn and Li through sulfate decomposition roasting followed by water leaching, and obtain a pure leachate with low content of Al and Si which is beneficial to the production of Li chemicals [27].

Table 2 Possible reactions between manganese-rich slag and H_2SO_4 during roasting

Reaction	No.
$MnAl_2O_4+4H_2SO_4=MnSO_4+Al_2(SO_4)_3+4H_2O(g)$	(2)
$MnAl_2O_4+4H_2SO_4=MnSO_4\cdot H_2O+Al_2(SO_4)_3+3H_2O(g)$	(3)
$MgAl_2O_4+4H_2SO_4=MgSO_4+Al_2(SO_4)_3+4H_2O(g)$	(4)
$Mn_2SiO_4+2H_2SO_4=2MnSO_4+H_4SiO_4$	(5)
$Mn_2SiO_4+2H_2SO_4+2H_2O(l)=2MnSO_4\cdot H_2O+H_4SiO_4$	(6)
$2LiAlSiO_4+4H_2SO_4=Li_2SO_4+Al_2(SO_4)_3+2H_4SiO_4$	(7)
$Al_2(SO_4)_3=Al_2O_3+3SO_3(g)$	(8)
$H_4SiO_4(a)=SiO_2+2H_2O(g)$	(9)
$MnSO_4=MnO+SO_3(g)$	(10)
$MnSO_4\cdot H_2O=MnO+SO_3(g)+H_2O(g)$	(11)
$Li_2SO_4=Li_2O+SO_3(g)$	(12)

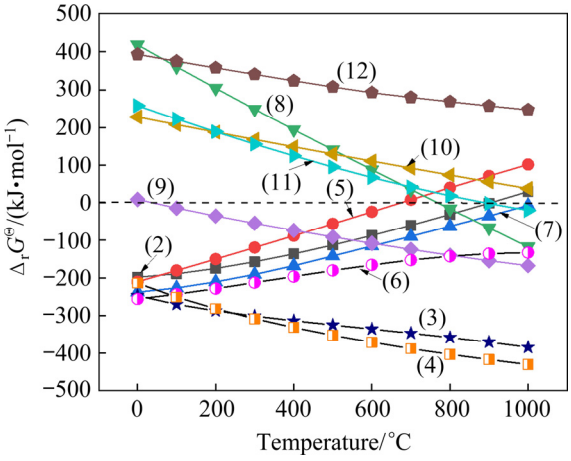

Fig. 3 Δ_rG^{Θ}−T relation diagram of possible chemical reactions between manganese-rich slag and H_2SO_4 during roasting

According to Reactions (2)−(5), it seems that the elements of Al and Si in the manganese-rich slag would consume plenty of H_2SO_4 due to the formation of $Al_2(SO_4)_3$ and H_4SiO_4. However, the H_2SO_4 can be regenerated by absorbing the SO_3 gas released from the decomposition of $Al_2(SO_4)_3$ at high temperature according to the following reaction:

$$SO_3(g)+H_2O(l)=H_2SO_4(l) \quad (13)$$

3.2.2 Phase evolution during roasting process

Figure 4 shows the XRD patterns of the manganese-rich slag and calcines obtained at different roasting temperatures. As observed in Fig. 4(a), the manganese-rich slag mainly consisted of Mn_2SiO_4 (tephroite), $LiAlSiO_4$ (pseudoeucrytite), and $Mn(Mg)Al_2O_4$ (spinel). After roasting with concentrated sulfuric acid at 200 °C, the diffraction peaks of the crystal phase containing lithium, $LiAlSiO_4$, disappeared completely; as a result, a very high leaching efficiency of lithium was obtained (Fig. 2(b)). Although the diffraction peaks of the crystal phase containing manganese (tephroite, Mn_2SiO_4) disappeared completely, the phase of spinel containing Mn was still detected. This is the reason why the leaching efficiency of Mn was lower than that of Li at a roasting temperature of 200 °C.

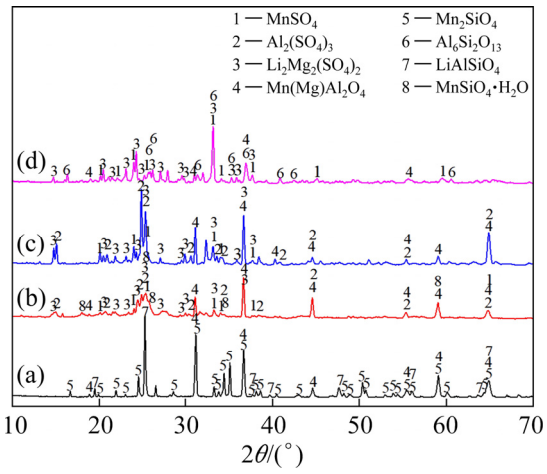

Fig. 4 XRD patterns of manganese-rich slag (a) and calcines at different roasting temperatures: (b) 200 °C; (c) 500 °C; (d) 800 °C

As the roasting temperature increased from 200 to 500 °C, the diffraction intensities of the spinel were significantly weakened (2θ=44.69°, 58.98°), while the $Al_2(SO_4)_3$ peak intensities were enhanced (2θ=15.19°, 24.99°). This outcome is ascribed to the fact that $Al_2(SO_4)_3$ was generated with the decomposition of the spinel phase. However, the lowest leaching efficiencies of Mn and Li were observed under this condition, which may be ascribed to the absorption by $Al(OH)_3$ gel, resulting from the hydrolysis of $Al_2(SO_4)_3$ during the water leaching process.

When the roasting temperature reached up to 800 °C, the mullite ($Al_6Si_2O_{13}$) peaks were first observed, which results from the reaction between SiO_2 and intermediate products of $Al_2(SO_4)_3$ decomposition. These phase conversion processes might be illustrated by Equations (14)−(16):

$$Al_2(SO_4)_3=Al_2O_3+3SO_3(g) \quad (14)$$

$$H_4SiO_4=SiO_2+2H_2O(g) \quad (15)$$

$$3Al_2O_3+2SiO_2=Al_6Si_2O_{13} \quad (16)$$

The formation of mullite effectively decreased the leaching efficiencies of Al and Si, and avoided the problem of filtration by $Al(OH)_3$ and silica gel, while increasing the Li leaching efficiency. However, the leaching efficiency of Mn was still lower than that at the roasting temperature of 200 °C. This is due to the regeneration of the spinel bearing Mn. The relevant reaction can be written as follows:

$$Al_2O_3+MnSO_4+H_2O=MnO\cdot Al_2O_3+H_2SO_4(l) \quad (17)$$

In order to ascertain unleachable phases, the leaching residue of the manganese-rich slag roasted at 800 °C was analyzed by XRD (Fig. 5). It is shown that $Al_6Si_2O_{13}$ and $Mn(Mg)Al_2O_4$ remain in the leaching residue, resulting in a limitation on increasing Mn extraction further.

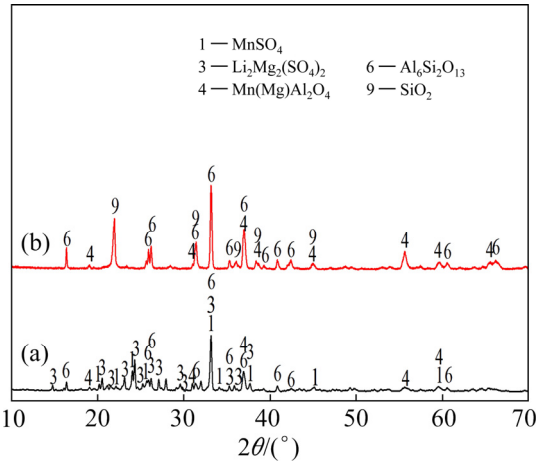

Fig. 5 XRD patterns of calcines (a) and leaching residue (b)

3.2.3 Thermal analysis of roasting process

Figure 6 displays the TG−DSC curves of the manganese-rich slag−H_2SO_4 mixture. As shown in Fig. 6, with the temperature increasing from room temperature to about 200 °C, two pronounced endothermic peaks were observed at approximately 116 and 198 °C in connection with 15.03% of the mass loss, which could be assigned to the volatilization of water and the formation of sulfates such as Mn, Li and Al according to Reactions (2)−(4) [28]. As a result, the leaching efficiencies of Mn, Li and Al should have reached a higher level at a roasting temperature of about 200 °C, which has been confirmed by the experimental results. As the temperature increased further, there were three puny exothermic peaks at 312, 571 and 619 °C which could be attributed to the decomposition of H_4SiO_4 and the formation of spinel, respectively. When the temperature reached 715 °C, an obvious endotherm peak was observed. This peak is mainly attributed to the decomposition of $Al_2(SO_4)_3$ [29,30]. This implies that the roasting temperature should be higher than 715 °C in order to decrease the Al leaching efficiency efficiently, which is in agreement with the XRD results. The endothermic peak presented at 874 °C is contributed by the decomposition of $MnSO_4$. Thus, the roasting temperature should be controlled at a lower temperature than about 874 °C.

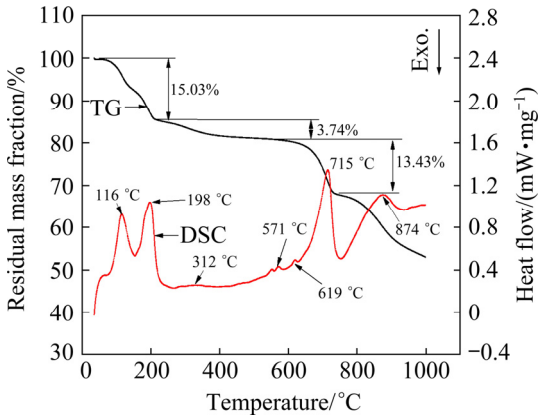

Fig. 6 DSC−TG curve of manganese-rich slag mixed with H_2SO_4

3.2.4 Microstructure of calcines

Figure 7 shows the SEM images of cross sections of sinters obtained under different conditions. As roasting temperature increased from 500 to 800 °C, crystal spinel particles were easily observed, and the size of their particles increased significantly (Table 3). This may be explained that, in spite of the filter problem being solved, the leaching efficiencies of Mn and Li still decreased. With increasing the roasting time from 2 to 4 h at

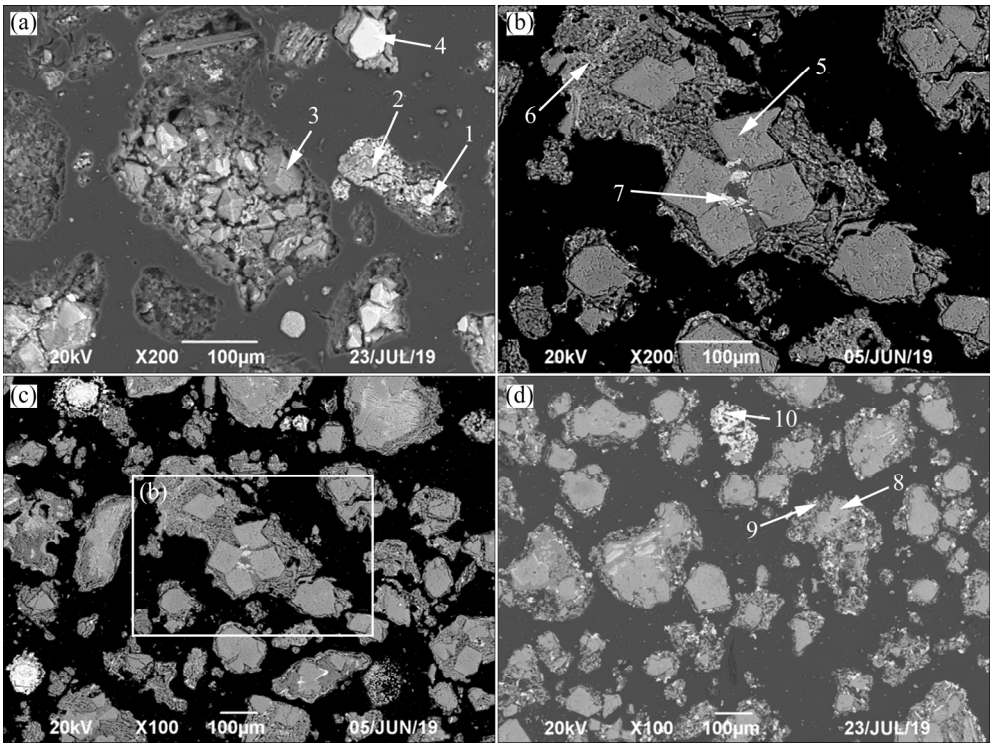

Fig. 7 SEM images showing cross sections of sinters obtained under different conditions: (a) 500 °C for 2 h; (b, c) 800 °C for 2 h; (d) 800 °C for 6 h

800 °C, the size of spinel particles increased significantly. This further confirms that the formation of spinel particles resulted in the loss of Mn and Li, which is in accordance with the results of the roasting−water leaching, as shown in Fig. 2(b).

Figure 8 depicts a schematic representation during the sulfation roasting−water leaching process. During the roasting process, the manganese-rich slag first reacted with concentrated sulfuric acid, producing $MnSO_4$, $MnSO_4·H_2O$, $Li_2Mg(SO_4)_2$, $Al_2(SO_4)_3$, and H_4SiO_4. It should be mentioned that the Mg in $Li_2Mg(SO_4)_2$ was obtained from the slag maker during the production of Mn-rich slag [7,16,17]. As the roasting temperature increased, the H_4SiO_4 and $Al_2(SO_4)_3$ decomposed successively, resulting in the formation of mullite and spinel. The formation of mullite aided in decreasing the leaching efficiencies of Al and Si, while improving the leaching efficiency of Li. The formation of spinel, on the other hand, reduced the leaching efficiencies of Mn and Li. During the roasting process, SO_3-bearing tail gas was released, which can be absorbed and converted back to H_2SO_4 according to Reaction (13). As a

Table 3 EDS analysis results of selected sinters in Fig. 7 (wt.%)

Area	O	Na	Mg	Al	Si	S	K	Ca	Mn	Fe	Ni
1	4.00		4.75	57.48		0.61			33.16		
2	2.96			8.32	11.85	42.48	15.84	2.00	16.55		
3	7.27			14.59	54.02	11.90	2.13		10.09		
4	3.75		4.82	57.42					34.01		
5	4.38		5.18	57.64					32.80		
6		0.51	0.40	1.67	44.77	24.67	3.89	4.85	16.49	2.15	0.60
7	1.48			2.37	2.50	2.60	0.71		6.51	83.83	
8	4.12		5.22	58.46					32.20		
9	2.98			5.70	26.57	23.63	3.96	21.70	11.20	4.26	
10	2.23			4.38	11.00				82.39		

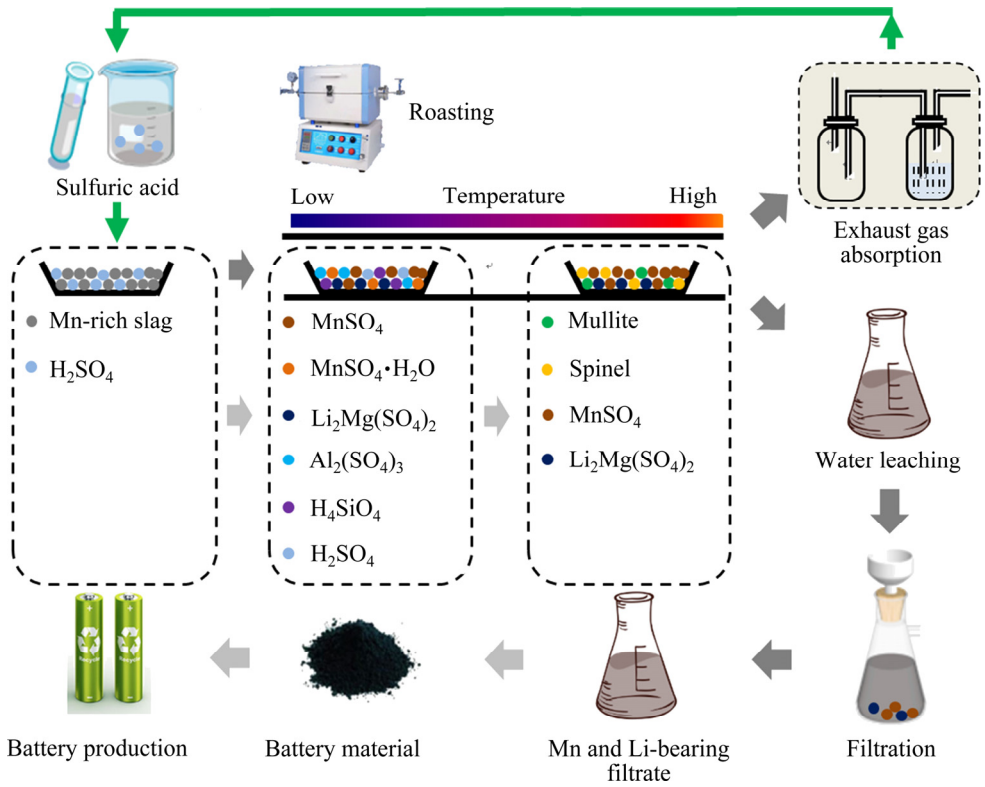

Fig. 8 Schematic diagram of evolutions of main elements during sulfation roasting−water leaching process

result, the actual H_2SO_4 consumption is very low, and no waste gas is produced. The tail gas absorption device can be found in the study by LI et al [30]. By referring to the studies of WENG et al [31], LI et al [32], and NIE et al [33], the Mn and Li-bearing filtrate can be used to produce $LiMn_2O_4$, $Li[(Ni_{1/3}Co_{1/3}Mn_{1/3})_{1-x}Mg_x]O_2$, $ZnMn_2O_4$ and $Li_{0.25}Na_{0.6}MnO_2$ battery materials. Thus, the proposed technique has advantages in terms of cleanliness and economics, as well as a lower H_2SO_4 composition and no waste gas generation.

4 Conclusions

(1) The leaching efficiencies of Mn and Li were significantly affected by the roasting temperature and time. Their leaching efficiencies decreased significantly with the increase in roasting temperature between 200 and 500 °C, but they increased dramatically when the roasting temperature went beyond 500 °C. The leaching efficiency of Mn decreased significantly with the roasting time increasing.

(2) The optimum roasting conditions were: acid concentration of 82 wt.%, acid-to-slag mass ratio of 1.5:1, roasting temperature of 800 °C, and roasting time of 2 h. Under these conditions, the leaching efficiencies of Mn and Li reached 73.71% and 73.28%, respectively.

(3) During the roasting process, the manganese-rich slag first reacted with concentrated sulfuric acid, producing $MnSO_4$, $MnSO_4·H_2O$, $Li_2Mg(SO_4)_2$, $Al_2(SO_4)_3$, and H_4SiO_4. As the roasting temperature increased, H_4SiO_4 and $Al_2(SO_4)_3$ decomposed successively, resulting in generations of mullite and spinel. The formation of mullite was beneficial to decreasing the leaching efficiencies of Al and Si, while increasing the leaching efficiency of Li. The formation of spinel, however, decreased the leaching efficiencies of Mn and Li.

Acknowledgments

This work was supported by the National Natural Science Foundation of China (No. 51704038), the State-Owned Enterprise Electric Vehicle Industry Alliance, China (No. JS-211), and the Changsha Science and Technology Project, China (No. kq1602212).

References

[1] HE Shi-chao, LIU Zhi-hong. Efficient process for recovery of waste $LiMn_2O_4$ cathode material precipitation thermodynamic analysis and separation experiments [J]. Waste Management, 2020, 113: 105−117.

[2] FENG Ting-ting, YANG Jian, DAI Si-yi, WANG Jun-chao, WU Meng-qiang. Microemulsion synthesis of $ZnMn_2O_4$/Mn_3O_4 sub-microrods for Li-ion batteries and their conversion reaction mechanism [J]. Transactions of Nonferrous Metals Society of China, 2021, 31: 265−276.

[3] QU Xin, XIE Hong-wei, CHEN Xiang, TANG Yi-qi, ZHANG Bei-lei, XING Peng-fei, YIN Hua-yi. Recovery of $LiCoO_2$ from spent lithium-ion batteries through a low-temperature ammonium chloride roasting approach: Thermodynamics and reaction mechanisms [J]. ACS Sustainable Chemistry Engineering, 2020, 8: 6524−6532.

[4] DAŃCZAK A, KLEMETTINEN L, KURHILA M, TASKINEN P, LINDBERG D, JOKILAAKSO A. Behavior of battery metals lithium, cobalt, manganese and lanthanum in black copper smelting [J]. Batteries, 2020, 6: 16.

[5] LU Shi-jie, LIU Yang, HE Zhen-jiang, LI Yun-jiao, ZHENG Jun-chao, MAO Jing, DAI Ke-hua. Synthesis and properties of single-crystal Ni-rich cathode materials in Li-ion batteries [J]. Transactions of Nonferrous Metals Society of China, 2021, 31: 1074−1086.

[6] LIU Fu-peng, PENG Chao, MA Quan-xin, WANG Jin-liang, ZHOU Song-lin, CHEN Zao-ming, WILSON B P, LUNDSTROM M. Selective lithium recovery and integrated preparation of high-purity lithium hydroxide products from spent lithium-ion batteries [J]. Separation Purification Technology, 2021, 259: 118181.

[7] XIAO Song-wen, REN Guo-xing, XIE Mei-qiu, PAN Bing, FAN You-qi, WANG Feng-gang, XIA Xing. Recovery of valuable metals from spent lithium-ion batteries by smelting reduction process based on $MnO−SiO_2−Al_2O_3$ slag system [J]. Journal of Sustainable Metallurgy, 2017, 3(4): 703−710.

[8] REN Guo-xing, XIAO Song-wen, XIE Mei-qiu, PAN Bing, CHEN Jian, WANG Feng-gang, XIA Xing. Recovery of valuable metals from spent lithium ion batteries by smelting reduction process based on $FeO−SiO_2−Al_2O_3$ slag system [J]. Transactions of Nonferrous Metals Society of China, 2017, 27: 450−456.

[9] LEI Shu-ya, XU Rui, SUN Wei, XU Sheng-ming, YANG Yue. Recycling of spent lithium-ion battery [J]. The Chinese Journal of Nonferrous Metals, 2021, DOI: 10.11817/j.ysxb.1004.0609.201-42256. (in Chinese)

[10] YANG Jian, QIN Ji-tao, LI Fang-cheng, JIANG Liang-xing, LAI Yan-qing, LIU Fang-yang, JIA Ming. Review of hydrometallurgical processes for recycling spent lithium-ion batteries [J]. Journal of Central South University (Science and Technology), 2020, 51(12): 3261−3268. (in Chinese)

[11] MURAKAMI Y, MATSUZAKI Y, KAMIMURA T, NISHIURA T, MASUDA K, SHIBAYAMA A, INOUE R. Erosion mechanism of refractories in a pyro-processing furnace for recycling lithium-ion secondary batteries [J]. Ceramics International, 2020, 46: 9281−9288.

[12] MAKUZA B, TIAN Qing-hua, GUO Xue-yi, CHATTOPADHYAY K, YU Da-wei. Pyrometallurgical options for recycling spent lithium-ion batteries: A comprehensive review [J]. Journal of Power Sources, 2021, 491: 229622.

[13] HU Xian-feng, MOUSA E, YE Guo-zhu. Recovery of Co, Ni, Mn, and Li from Li-ion batteries by smelting reduction. Part II: A pilot-scale demonstration [J]. Journal of Power Sources, 2021, 483: 229089.

[14] GEORGI-MASCHLER T, FRIEDRICH B, WEYHE R, HEEGN H, RUTZ M. Development of a recycling process for Li-ion batteries [J]. Journal of Power Sources, 2012, 207: 173−182.

[15] KLIMKO J, ORÁČ D, MIŠKUFOVÁ A, VONDERSTEIN C, DERTMANN C, SOMMERFELD M, FRIEDRICH B, HAVLÍK T. A combined pyro- and hydrometallurgical approach to recycle pyrolyzed lithium-ion battery black mass. Part 2: Lithium recovery from Li enriched slag-thermodynamic study, kinetic study, and dry digestion [J]. Metals, 2020, 10: 1558.

[16] REN Guo-xing, XIAO Song-wen, XIE Mei-qiu, PAN Bing, FAN You-qi, WANG Feng-gang, XIA Xing. Recovery of valuable metals from spent lithium-ion batteries by smelting reduction process based on $MnO-SiO_2-Al_2O_3$ slag system [C]//Advances in Molten Slags, Fluxes, and Salts: Proceedings of the 10th International Conference on Molten Slags, Fluxes and Salts. Seattle, USA: WILEY, 2016: 211−218.

[17] REN Guo-xing, XIAO Song-wen, XIA Long-gong, LIAO Cai-bin, LIU Zhi-hong. The distribution of cobalt between Co−Cu alloys and alumina-saturated $MnO-SiO_2-Al_2O_3$ slags [J]. Metallurgical and Materials Transactions B, 2021, 52B: 314−321.

[18] HANISCH C, DIEKMANN J, STIEGER A, HASELRIEDER W, KWADE A. Recycling of lithium-ion batteries [C]//Handbook of Clean Energy Systems. John Wiley & Sons, Ltd., 2015: 1−24.

[19] SCHWICH L, SCHUBERT T, FRIEDRICH B. Early-stage recovery of lithium from tailored thermal conditioned black mass. Part I: Mobilizing lithium via supercritical CO_2-carbonation [J]. Metals, 2021, 11: 177.

[20] HOLZER A, WINDISCH-KERN S, PONAK C, RAUPENSTRAUCH H. A novel pyrometallurgical recycling process for lithium-ion batteries and its application to the recycling of LCO and LFP [J]. Metals, 2021, 11: 149.

[21] DANG Hui, WANG Ben-feng, CHANG Zhi-dong, WU Xue, FENG Jing-ge, ZHOU Hua-lei, LI Wen-jun, SUN Chang-yan. Recycle lithium from simulated pyro-metallurgical slag by chlorination roasting [J]. ACS Sustainable Chemistry Engineering, 2018, 6(10): 13160−13167.

[22] DANG Hui, LI Na, CHANG Zhi-dong, WANG Ben-feng, ZHAN Yi-fei, WU Xue, LIU Wen-bo, ALI S, LI Hong-da, GUO Jia-hui, LI Wen-jun, ZHOU Hua-lei, SUN Chang-yan. Lithium leaching via calcium chloride roasting from simulated pyrometallurgical slag of spent lithium ion battery [J]. Separation and Purification Technology, 2020, 233: 116025.

[23] LI Na, GUO Jia-hui, CHANG Zhi-dong, DANG Hui, ZHAO Xin, ALI S, LI Wen-jun, ZHOU Hua-lei, SUN Chang-yan. Aqueous leaching of lithium from simulated pyro-metallurgical slag by sodium sulfate roasting [J]. RSC Advances, 2019, 9: 23908−23915.

[24] GAINES L. Lithium-ion battery recycling processes: Research towards a sustainable course [J]. Sustainable Materials Technologies, 2018, 17: e00068.

[25] DUAN Xue-ke, ZHENG Han, CHEN Yong-qiang, QIAN Fan, LIU Guo-qi, WANG Xin-fu, SI Yao-chen. Study on the corrosion resistance of cordierite−mullite and SiC refractories to Li-ion ternary cathode materials [J]. Ceramics International, 2020, 46: 2829−2835.

[26] RUISMÄKI R, RINNE T, DAŃCZAK A, TASKINEN P, SERNA-GUERRERO R, JOKILAAKSO A. Integrating flotation and pyrometallurgy for recovering graphite and valuable metals from battery scrap [J]. Metals, 2020, 10: 680.

[27] ZHANG Jia-liang, HU Jun-tao, LIU Yu-bo, JING Qian-kun, YANG Cheng, CHEN Yong-qiang, WANG Cheng-yan. Sustainable and facile method for the selective recovery of lithium from cathode scrap of spent $LiFePO_4$ batteries [J]. ACS Sustainable Chemistry Engineering, 2019, 7(6): 5626−5631.

[28] TENG Ai-jun, XUE Xiang-xin. A novel roasting process to extract vanadium and chromium from high chromium vanadium slag using a $NaOH-NaNO_3$ binary system [J]. Journal of Hazardous Materials, 2019, 379: 120805.

[29] ZHANG Chang-da, HU Bin, WANG Hua-guang, WANG Min-yu, WANG Xue-wen. Recovery of valuable metals from copper slag [J]. Mining Metallurgy Exploration, 2020, 37: 1241−1251.

[30] LI Peng-wei, LUO Shao-Hua, FENG Jian, LV Fang, YAN Sheng-xue, WANG Qing, ZHANG Ya-hui, MU Wen-ning, LIU Xin, LEI Xue-Fei, TENG Fei, LI Xian, CHANG Long-jiao, LIANG Jin-sheng, DUAN Xin-hui. Study on the high-efficiency separation of Fe in extracted vanadium residue by sulfuric acid roasting and the solidification behavior of V and Cr [J]. Separation and Purification Technology, 2021, 269: 118687.

[31] WENG Ya-qing, XU Sheng-ming, HUANG Guo-yong, JIANG Chang-yin. Synthesis and performance of $Li[(Ni_{1/3}Co_{1/3}Mn_{1/3})_{1-x}Mg_x]O_2$ prepared from spent lithium ion batteries [J]. Journal of Hazardous Materials, 2013, 246/247: 163−172.

[32] LI Peng-wei, LUO Shao-hua, WANG Qing, ZHANG Ya-hui, LIU Xin, XU Cai-hong, LIANG Jin-sheng, DUAN Xin-hui. Hydrothermal synthesis of nano spheroid-like $ZnMn_2O_4$ materials as high-performance anodes for lithium-ion batteries [J]. International Journal of Energy Research, 2021, 45(12): 18081−18090.

[33] NIE Xue-jiao, GUO Jin-zhi, WANG Mei-yi, GU Zhen-yi, ZHAO Xin-xin, YANG Xu, LIANG Hao-jie, WU Xing-long. Using spent lithium manganate to prepare $Li_{0.25}Na_{0.6}MnO_2$ as cathode material in sodium-ion batteries [J]. Energy Storage Science and Technology, 2020, 9(5): 1402−1409. (in Chinese)

废旧锂离子电池火法冶炼富锰渣中锰和锂的提取

任国兴[1], 廖财斌[2], 刘志宏[1], 肖松文[2]

1 中南大学 冶金与环境学院，长沙 410083;
2 长沙矿冶研究院有限责任公司，长沙 410012

摘　要：开展富锰渣硫酸化焙烧−水浸选择性提取锰和锂的试验，采用 XRD、TG−DSC 和 SEM−EDS 详细分析锰和锂的提取机理。结果表明，在酸浓度为 82%(质量分数)、酸矿质量比 1.5:1、焙烧温度 800 ℃和焙烧时间 2 h 时，Mn 和 Li 的浸出率分别达到 73.71%和 73.28%。焙烧过程中，富锰渣首先与浓硫酸反应形成 $MnSO_4$、$MnSO_4·H_2O$、$Li_2Mg(SO_4)_2$、$Al_2(SO_4)_3$ 和 H_4SiO_4。随着焙烧温度的升高，H_4SiO_4 和 $Al_2(SO_4)_3$ 依次分解，并形成莫来石和尖晶石相。莫来石的形成有利于降低 Al 和 Si 的浸出率而增加 Li 的浸出率；而尖晶石的形成则会降低 Mn 和 Li 的浸出率。

关键词：废旧锂离子电池；富锰渣；硫酸化焙烧；锰回收；锂回收

(Edited by Bing YANG)